Methyltransferase-like 7B promotes M2-like macrophage polarization in lung adenocarcinoma via upregulating human epidermal growth factor receptor 3 expression and secretion

SIXIAO HE[1*], HUIBIN SONG[2,3*], JIE WU[4], JINQUAN XIA[5], NI LIU[6], JIA CAO[7], ZIXUAN ZHANG[8], XIAOLIN CUI[1] and CHANG ZOU[1,9]

[1]School of Medicine, The Chinese University of Hong Kong, Shenzhen, Guangdong 518020, P.R. China; [2]Department of Thoracic Surgery, Shenzhen People's Hospital (The First Affiliated Hospital, Southern University of Science and Technology; The Second Clinical Medical College, Jinan University), Shenzhen, Guangdong 518020, P.R. China; [3]The First Affiliated Hospital, School of Medicine, Southern University of Science and Technology, Shenzhen, Guangdong 518055, P.R. China; [4]Department of Pharmacy, Chaozhou Central Hospital, Chaozhou, Guangdong 521000, P.R. China; [5]Department of Central Laboratory, Shenzhen People's Hospital (The Second Clinical Medical College), Jinan University, The First Affiliated Hospital of Southern University of Science and Technology, Shenzhen, Guangdong 518020, P.R. China; [6]School of Public Health, University of South China, Hengyang, Hunan 421001, P.R. China; [7]School of Basic Medical Sciences, University of South China, Hengyang, Hunan 421001, P.R. China; [8]Department of Oncology, Affiliated Hospital of Guangdong Medical University, Zhanjiang, Guangdong 524000, P.R. China; [9]Department of Central Laboratory, Shenzhen People's Hospital (The First Affiliated Hospital, Southern University of Science and Technology; The Second Clinical Medical College, Jinan University), Shenzhen, Guangdong 518020, P.R. China

Received June 4, 2026; Accepted September 4, 2026

DOI: 10.3892/ol.2026.15871

Abstract. M2-like tumor-associated macrophages form an immunosuppressive tumor microenvironment that drives tumor progression and limits therapeutic efficacy. Although methyltransferase-like 7B (METTL7B) acts as an oncogenic regulator of lung cancer, its non-cell-autonomous paracrine role in modulating macrophage polarization remains poorly characterized. In the present study, a public single-cell RNA sequencing dataset (GSE131907) and The Cancer Genome Atlas-Lung Adenocarcinoma (LUAD) cohort were integrated for bioinformatics screening and validation was performed using stable METTL7B-knockout A549 and METTL7B-overexpressing PC9 cell models. METTL7B was predominantly enriched in LUAD malignant epithelial cells and was positively correlated with human epidermal growth factor receptor 3 (ERBB3) expression. METTL7B upregulated both full-length and soluble ERBB3 isoforms and the METTL7B-induced elevation of ERBB3 ectodomain release was dependent on ADAM metallopeptidase domain 10/17-mediated proteolytic cleavage. Functionally, METTL7B promoted macrophage recruitment and induced functional M2 polarization via the soluble ERBB3 extracellular domain (ECD), with EGFR acting as the candidate receptor. Rescue and inhibition assays demonstrated that the ERBB3-EGFR axis mediated METTL7B-driven macrophage reprogramming. Clinically, the expression of both METTL7B and ERBB3 progressively increases with LUAD histological progression. The present findings delineate a novel METTL7B-ERBB3-ECD-EGFR paracrine axis in tumor-macrophage crosstalk, providing a potential therapeutic target for LUAD.

Correspondence to: Professor Chang Zou or Professor Xiaolin Cui, School of Medicine, The Chinese University of Hong Kong, 2001 Longxiang Avenue, Shenzhen, Guangdong 518020, P.R. China
E-mail: zouchang@cuhk.edu.cn
E-mail: stevencui@cuhk.edu.cn

*Contributed equally

Abbreviations: METTL7B, methyltransferase-like 7B; ERBB3, human epidermal growth factor receptor 3; TCGA, The Cancer Genome Atlas; LUAD, lung adenocarcinoma; TAMs, tumor-associated macrophages; ECD, extracellular domain; IHC, immunohistochemistry; ELISA, enzyme-linked immunosorbent assay

Key words: METTL7B, ERBB3; M2 macrophage polarization, lung adenocarcinoma, tumor microenvironment

Introduction

Lung adenocarcinoma (LUAD) is the most common histological subtype of non-small cell lung cancer (NSCLC) and remains the leading cause of cancer-associated mortality worldwide, accounting for ~40% of all lung cancer cases (1,2). Despite the advances in molecular targeted therapy and immune checkpoint blockade regimens, the long-term clinical survival of patients with LUAD remains unsatisfactory (3-5). A key driver of treatment failure is the immunosuppressive tumor microenvironment (TME), which protects malignant

cells and impairs antitumor immunity (6-9). As the most abundant myeloid population within the TME, tumor-associated macrophages (TAMs) exhibit high functional plasticity (6,10). Malignant cells frequently 're-educate' TAMs toward an M2-like phenotype (11), which suppresses T-cell cytotoxicity (12) and promotes angiogenesis (13), thereby facilitating tumor progression and immune evasion (14,15).

Methyltransferase-like 7B (METTL7B) is a member of the METTL protein family recognized for its diverse regulatory roles in human malignancies (16). A previous study identified METTL7B as a key oncogenic driver in lung cancer, essential for NSCLC cell proliferation and tumorigenesis (17), and as potential therapeutic target for reversing EGFR-tyrosine kinase inhibitors resistance in LUAD (18). However, the aforementioned studies have focused primarily on the cell-autonomous effects of METTL7B in tumor cell survival and therapeutic resistance. Whether METTL7B exerts non-cell-autonomous effects to orchestrate tumor-myeloid crosstalk, particularly by driving M2 macrophages polarization, remains unclear.

Human epidermal growth factor receptor 3 (ERBB3), also known as HER3, is a member of the human EGFR/ErbB family of receptor tyrosine kinases (19,20), and is a catalytically inactive pseudokinase that transduces signals via heterodimerization with other family members (21). Accumulating evidence has demonstrated that ERBB3 drives oncogenic bypass signaling and therapeutic resistance and is emerging as a novel antibody-drug conjugate (ADCs) target (22-25). Several ERBB3-targeted ADCs, including patritumab, deruxtecan and BL-B01D1, are under early clinical evaluation for LUAD with promising therapeutic potential, as they have demonstrated objective antitumor responses in heavily pretreated patients with advanced solid tumors (26). Beyond its canonical role as a transmembrane receptor, ERBB3 can exist as a secreted isoform (sHER3) or a soluble extracellular domain (ECD) generated via alternative splicing or proteolytic shedding (27). Although membrane-bound ERBB3 is a well-documented driver of cell-intrinsic survival (28,29), the paracrine roles of ERBB3-ECD in the TME, especially in modulating immune cells, remain largely elusive. Other ErbB family receptors, particularly EGFR, are functionally expressed in macrophages (30) and mediate paracrine signal transduction in the TME (31). Nevertheless, whether soluble ERBB3-ECD communicates with macrophage EGFR to regulate immune polarization and whether this signaling cascade is controlled by upstream METTL7B remains uncharacterized.

In the present study, single-cell RNA-sequencing (scRNA-seq) data from the public GSE131907 dataset were integrated with large-scale The Cancer Genome Atlas (TCGA)-LUAD transcriptomic datasets to identify potential associations between METTL7B and ERBB3 in malignant epithelial cells. *In vitro* functional validation, ADAM metallopeptidase domain (ADAM) protease inhibition, receptor blockade and cytokine profiling were combined to characterize the tumor-immune paracrine regulatory cascade. The present study aimed to explore whether METTL7B regulate macrophage M2-like reprogramming via ERBB3-ECD-EGFR paracrine signaling, and to uncover its non-cell autonomous oncogenic mechanism in LUAD, so as to identify potential therapeutic targets.

Materials and methods

Ethics statement. A total of six formalin-fixed paraffin-embedded LUAD tissue specimens, spanning minimally invasive adenocarcinoma (MIA), invasive adenocarcinoma (IA) and lung adenocarcinoma (LUAD), were obtained from Shenzhen People's Hospital (Shenzhen, China). Samples were retrospectively accessed from archived pathology specimens collected between January and February 2025. The inclusion criteria were: i) Histologically confirmed lung adenocarcinoma (including MIA and IA); available formalin fixed paraffin embedded tissue blocks; complete clinical pathological information. Exclusion criteria were: i) Patients with prior anti-tumor therapy before surgical resection; insufficient tumor tissue for experiments. For the entire patient cohort (n=6), there were 3 men and 3 women. The median age was 59 years, and the ages ranged from 52 to 68 years. Demographic details for each subgroup are listed below: i) LUAD group: 1 male (68 years old) and 1 female (63 years old); ii) IA group: 1 male (52 years old) and 1 woman (61 years old); and (iii) MIA group: 1 man (54 years old) and 1 female (57 years old).

The present study was conducted in accordance with the Declaration of Helsinki and approved by the Clinical Research Ethics Committee of Shenzhen People's Hospital (approval no. LL-KY-2024161-01; approval date: 2024-10-18). The ethical approval covers the written informed consent obtained from all participants, which authorizes the use of their residual surgically resected lung cancer tissues.

Bioinformatics analysis. Publicly available transcriptomic datasets were retrieved for the integrated analysis. Bulk RNA-seq data and corresponding clinical information of TCGA-LUAD cohort were downloaded from the UCSC Xena browser (https://xenabrowser.net/). For scRNA-seq analysis, the raw counts of the GSE131907 dataset (32) were obtained from the Gene Expression Omnibus (GEO) database (https://www.ncbi.nlm.nih.gov/geo/). In total, 11 LUAD tumor specimens were included. All data were normalized and log-transformed, as appropriate, prior to downstream analysis. For differential expression and functional enrichment analyses, adjusted P-value <0.05 was defined as the significance cut-off level.

scRNA-seq analysis. The raw and processed counts for the scRNA-seq analysis were obtained from the GEO repository under accession number GSE131907. Specifically, a subset of 11 tumor tissue specimens was utilized (LUNG_T06, LUNG_T08, LUNG_T09, LUNG_T18, LUNG_T19, LUNG_T20, LUNG_T25, LUNG_T28, LUNG_T30, LUNG_T31 and LUNG_T34), corresponding to sample IDs GSM3827125 through GSM3827135.

The scRNA-seq data were processed using the Seurat R package (v4.0; satijalab.org/seurat/). Quality control was performed by filtering out cells with <200 or >6,000 detected genes; and >20% mitochondrial gene expression. After normalization and identification of highly variable genes, principal component analysis was performed for dimensionality reduction. Cells were clustered using the 'FindClusters' function and visualized using t-distributed stochastic neighbor embedding (t-SNE) or Uniform Manifold Approximation and Projection. The cell types were annotated based on the

expression of canonical markers, including CCL5, NKG7 and TRAC for T cells; CCL18, CD163 and CD68 for macrophages; SFTPA2 and SFTPC for epithelial cells; CD79A, MS4A1 and VPREB3 for B cells; G0S2, IL1B and S100A9 for monocytes; TPSB2, TPSAB1 and CPA3 for mast cells; MGP, DCN and LUM for fibroblasts; IGLC2, IGKC and IGLC3 for plasma cells; GNG11,RAMP2 and CCL21 for endothelial cells; MARCKSL1, BIRC3 and TXN for dendritic cells (DC).

GO and KEGG analysis. Functional enrichment analyses for GO (geneontology.org/) and KEGG (genome.jp/kegg/) were implemented via the metascape web server (metascape.org/), Terms with adjusted P-value <0.05 were regarded as statistically significant.

Cell-cell communication analysis. CellChat (v1.1) (https://github.com/jinworks/CellChat) was used to investigate the intercellular crosstalk between malignant cells and the immune microenvironment. This analysis utilizes a curated database of signaling molecule interactions to predict the probability and strength of communication between cell clusters. Malignant cells were stratified into METTL7B-expressing (METTL7B expression >0) and METTL7B-non-expressing (METTL7B expression=0) groups based on raw gene expression values. The interaction weights between METTL7B-high malignant cells and M2-like macrophages was focused on. The signaling contributions of specific ligand-receptor pairs, particularly those involving the ERBB3 axis, were quantified and visualized using chord diagrams and bubble plots.

Bulk RNA-seq analysis and clinical correlation. Large-scale transcriptomic and clinical data for TCGA-LUAD cohort were retrieved from the UCSC Xena browser (https://xenabrowser.net/). In TCGA-LUAD cohort, patients were divided into high- and low-expression groups based on the median expression level of METTL7B. Gene set enrichment analysis was conducted to identify pathways significantly enriched in METTL7B-high patients using MSigDB hallmark gene sets. Furthermore, the correlation between METTL7B expression and macrophage infiltration scores was evaluated (calculated using the CIBERSORT (cibersort.stanford.edu) or TIMER algorithms (https://timer.cistrome.org).

Protein-protein interaction analysis. PPI network analysis was performed using the STRING database (https://cn.string-db.org/) to predict potential functional associations between proteins of interest. Interactions with a confidence score ≥0.7 were considered significant.

Cell lines and cell culture. Human LUAD cell lines A549 (cat. no. CC0202), PC9 (cat. no. CC0204) and U937 (cat. no. CC1601) were purchased from CEllCOOK (Cells were cultured in RPMI-1640 medium (Gibco; Thermo Fisher Scientific, Inc.) supplemented with 10% fetal bovine serum (AboRo) and 1% penicillin/streptomycin (Sangon Biotech Co., Ltd) at 37˚C in a humidified atmosphere with 5% CO_2. All cell lines used in the present study, including U937, A549 and PC9, were authenticated via short tandem repeat, DNA profiling prior to the experiments, and were routinely confirmed to be free of mycoplasma contamination.

Generation of stable METTL7B-modified cell lines. Stable cell lines with manipulated METTL7B expression were established using lentiviral systems. For knockout (KO) models, a CRISPR-Cas9 (Guangzhou Yuanjing Biotechnology Co., Ltd.; cat. no. YV-Cas-LV001-1000) approach was employed in A549 cells using the pLV-U6-gRNA1-METTL7B-puro recombinant plasmid (constructed from the pLV-U6-puro-Cas9 backbone) to co-express Cas9 and an sgRNA targeting METTL7B (5'-GTTCTACCCACCGGGCTGCA-3'). For overexpression (OE) models, the human METTL7B coding sequence was sub-cloned into the pLV-EF1a-Myc-Puro vector (Jiangyuan Biotechnology; cat. no. JY10013) to generate Myc-tagged fusion proteins in PC9 cells.

Lentiviral particles for both constructs were produced using the 2nd generation lentiviral system. Briefly, transfer plasmids together with psPAX2 (Jiangyuan Biotechnology (Nanjing, China), Cat. no. JY03029) and pMD2G (Jiangyuan Biotechnology (Nanjing, China), Cat. no. JY03027) were co-transfected into 293T cells (CELLCOOK, Cat. no. CC4002) in a 10 cm dish. For transfection, 10 μg transfer plasmid, 6 μg psPAX2, and 4 μg pMD2G were used at a plasmid ratio of 5:3:2. Transfection was performed at 37˚C for 6-8 h. Lentiviral supernatants were collected at 72 h post-transfection, filtered and used for cell infection at a MOI of 10. The target cells were transduced for 12 h, and fresh medium was replenished afterwards. At 48 h after transduction, puromycin selection was performed at 5 μg/ml, for stable pool generation; the maintenance puromycin concentration was 1 μg/ml. A549-KO efficiency was validated in expanded single cell clones via genomic sequencing and western blot, while PC9-Myc-METTL7B status was confirmed using western blot analysis.

LDH release assay. Cytotoxicity was assessed using the LDH) cytotoxicity detection kit (Beyotime, Cat. no. C0016) according to the manufacturer's instructions. Cell-culture supernatants (conditioned medium) were collected before soluble ERBB3 quantification. Relative LDH release was quantified in A549 and PC9 cells upon METTL7B knockout (KO) or overexpression (OE).

Preparation of conditioned medium (CM). Cells (A549-WT/KO and PC9-NC/METTL7B) were seeded into T75 flasks and grown to 85% confluence. The culture medium was replaced with 5% FBS medium for 48 h. The supernatant (CM) was then collected and centrifuged at 500 x g for 10 min at 4˚C to remove the debris. CM was used immediately or stored at -80˚C.

Macrophage induction and co-culture. The human acute monocytic leukemia U937 cells were induced into M0 macrophages by treatment with 100 nM phorbol 12-myristate 13-acetate (PMA; cat. no. 524400; Sigma-Aldrich; Merck KGaA) for 48 h. For polarization experiments, M0 macrophages were co-incubated with the indicated tumor CM (with or without inhibitors/proteins) for an additional 48 h before collection for flow cytometry or reverse transcription-quantitative PCR (RT-qPCR) analysis.

RNA extraction and RT-qPCR. Total RNA was isolated using TRIzol® reagent (cat. no. 15596026CN; Invitrogen;

Table I. Primer sequences.

Gene	Primer sequence (5'-3')
GAPDH forward	GTCTCCTCTGACTTCAACAGCG
GAPDH reverse	ACCACCCTGTTGCTGTAGCCAA
METTL7B forward	CCAGATAAAGGGGCTTACAGGAG
METTL7B reverse	TCAGCCATGCTCTTTGTCAGG
CCL2 forward	AGAATCACCAGCAGCAAGTGTCC
CCL2 reverse	TCCTGAACCCACTTCTGCTTGG
CSF-1 forward	TGCTGTTGTTGGTCTGTCTC
CSF-2 reverse	GGTAGCACACTGGATCTTTCAA
CD206 forward	TGATACCTGCGACAGTAAACGA
CD206 reverse	CTTGCAGTATGTCTCCGCTTC
CD163 forward	TCGCTCATCCCGTCAGTCA
CD163 reverse	CCGCTGTCTCTGTCTTCGCT
ARG-1 forward	ACTTAAAGAACAAGAGTGTGATGTG
ARG-1 reverse	GCATCCACCCAGATGACTCC
CD80 forward	GCTGGCTGGTCTTTCTCACT
CD80 reverse	GTCCGGTTCTTGTACTCGGG
CD86 forward	GTTTCATTCCCTGATGTTACGAG
CD86 reverse	GAGAAAGGTGAAGATAAAAGCCG
ERBB3-L forward	CCCGGGTTAGAGGAAGAGGA
ERBB3-L reverse	TAGGGGGATGAGGTGGACTG
ERBB3-S forward	AGGGACCCAGGTCTACGATG
ERBB3-S reverse	GCACCTTGGAAGAGGCACTTA

CCL2, chemokine C-C motif ligand 2; CSF, colony-stimulating factor; ARG-1, arginase 1; ERBB3, human epidermal growth factor receptor 3; ERBB3-L, full length ERBB3; ERBB3-S, soluble ERBB3.

Thermo Fisher Scientific, Inc.) and quantified using Nanodrop one (Thermo Fisher Scientific, Inc.). RNA (1 μg) was reverse-transcribed according to the manufacturer's instructions (cat. no. AE341-02; TransGen Biotech Co., Ltd.). qPCR was performed using the PerfectStart Green qPCR SuperMix kit (cat. no. AQ602-02-V2; TransGen Biotech Co., Ltd) on a Quantstudio5 system. The thermocycling conditions were as follows: initial denaturation at 94˚C for 30 s, followed by 42 cycles of 94˚C for 5 s and 60˚C for 30 sec. Relative mRNA levels were calculated using the $2^{-\Delta\Delta Cq}$ method (33) normalized to GAPDH. The primer sequences are listed in Table I.

Western blot analysis. Total protein was extracted using RIPA lysis buffer (Thermo Fisher,) supplemented with protease and phosphatase inhibitors. Protein concentrations were determined using the BCA Protein Assay Kit (cat. no. 23225; Thermo Fisher Scientific, Inc.). Twenty micrograms of protein were separated by 10% SDS-PAGE and transferred onto PVDF membranes (MilliporeSigma). After blocking with 5% non-fat milk in TBST (0.1% Tween-20) for 1 h at room temperature, the membranes were incubated overnight at 4˚C with primary antibodies against METTL7B (1:1,000; cat. no. 17001-1-AP; Proteintech Group, Inc.), ERBB3 (1:1,000; cat. no. 12708; Cell Signaling Technology, Inc.), Myc-Tag (1:1,000; cat. no. 9B11; Cell Signaling Technology, Inc.) and GAPDH (1:5,000; cat. no. 380626; Chengdu Zen-Bioscience Co., Ltd.).

Following three washes with TBST, the membranes were incubated with horseradish peroxidase (HRP)-conjugated secondary antibodies (1:5,000 cat. no. 7074; Cell Signaling Technology, Inc.) for 1 h at room temperature. Protein bands were visualized using enhanced chemiluminescence (ECL) reagents (cat. no. 34096; Thermo Fisher Scientific, Inc.) and captured by a ChemiDoc™ XRS+ Imaging System with Image Lab™ Software(Version 5.1) (Bio-Rad Laboratories, Inc.). GAPDH was used to normalize the data.

Enzyme-linked immunosorbent assay (ELISA). The concentration of secreted ERBB3 ECD in the CM was quantified using a human ERBB3 ELISA Kit (cat. no. CSB-EL007765HU; Cusabio Technology, LLC) and the concentrations of IL-10 (cat. no. SE50211; Proteintech Group, Inc.), TGF-β (cat. no. SE50233; Proteintech Group, Inc.), IL-12 (cat. no. SE50032; Proteintech Group, Inc.) and TNF-α (cat. no. SE50002; Proteintech Group, Inc.) were assessed using ELISA according to the manufacturer's instructions. Briefly, CM or the supernatant from macrophages was collected and centrifuged at 1,000 x g for 20 min at 4˚C to remove the cellular debris. Samples and standards were added to pre-coated microplates and incubated with biotin-conjugated antibodies, followed by incubation with HRP-conjugated avidin. The absorbance was measured at 450 nm using a BioTek Cytation 5 microplate reader (CYT5MPV; BioTek Instruments). The concentration of ERBB3-ECD, and IL-10, TGF-β, IL-12 and TNF-α was determined by interpolation from a standard curve using a four-parameter logistic regression and expressed as pg/ml.

Macrophage recruitment assay. Macrophage recruitment was assessed using 24-well Transwell inserts (8 μm pore size; MilliporeSigma). U937 cells ($1x10^5$ cells/well) were seeded in the upper chambers and differentiated into M0 macrophages using 100 nM PMA for 48 h 37˚C, followed by 12 h of serum-starvation. Subsequently, 600 μl of tumor-CM was added to the lower chamber as a chemoattractant. After 48 h migration, non-migrated cells were removed using cotton swabs. The migrated cells were fixed with 4% paraformaldehyde for 20 min, stained with 0.1% crystal violet for 15 min, both at room temperature, and imaged under bright-field illumination using a Leica DMI8 inverted microscope (DFC7000 T camera; Leica Microsystems). Recruited macrophages were quantified by averaging five randomly selected fields per insert using the LAS X software (Version 4.13, Leica Microsystems).

Flow cytometry. To evaluate macrophage polarization, the harvested cells were resuspended in ice-cold PBS. Subsequently, the cells were stained with fluorochrome-conjugated antibodies against, anti-CD86-FITC(cat. no. 374204;BioLegend,Inc.) and anti-CD206-PE-Cyanine7 (cat. no. 25-2069-42; eBioscience; Thermo Fisher Scientific, Inc.) for 30 min at 4˚C in the dark.

Next, 10 μg/ml neutralizing antibody (cat. no. 10001-RE10; Sino Biological) against EGFR was used to pretreat macrophages for 12 h at 37˚C before supplementing with CM.

After washing twice with PBS, data were acquired on a BD FACSMelody™ cell flow cytometer (BD Biosciences). A minimum of 10,000 events within the myeloid gate were recorded for each sample. Spectral overlap was corrected using single-stained compensation controls. Data analysis was performed using FlowJo™ software (version 10.8; BD Biosciences).

Immunohistochemistry (IHC) and quantification. Serial sections (4-μm) were deparaffinized in xylene and rehydrated using a graded ethanol series. Heat-induced antigen retrieval was performed using citrate buffer (pH 6.0). Endogenous peroxidase activity was quenched with 3% H_2O_2, followed by blocking non-specific binding with 5% BSA for 1 h at room temperature. Sections were then incubated with primary antibodies against METTL7B (1:200) and ERBB3 (1:200) overnight at 4˚C. Subsequently, the sections were incubated with HRP-conjugated secondary antibodies (1:2,000, Abcam, cat. no. ab205718) at room temperature for 1 h. Immunoreactivity was visualized using a DAB substrate kit (cat. no. ab64238; Abcam) and counterstained with hematoxylin for 1-2 min at room temperature. Finally, the sections were dehydrated and mounted using a neutral resin. To evaluate the correlation between METTL7B and ERBB3 expression, the positively stained areas were quantified. A total of five representative high-power fields were randomly selected per section and imaged using a Leica DMI8 microscope. Image analysis was performed using ImageJ software (Version 1.53t). After color deconvolution to isolate the DAB signal, a unified threshold was applied to all images to identify positive staining. The results were expressed as the mean area fraction (percentage of positive area) across the five fields for each specimen.

Reagents and inhibitors. The A549 and PC9 cell models were pretreated with the ADAM10/17 inhibitors GW280264X (cat. no. HY-115670; MedChemExpress) for 12 h, after which the CM was collected for ELISA. The specific ERBB3 inhibitor TX1-85-1(cat. no. HY-100848; MedChemExpress) was used at a final concentration of 5 μM. Recombinant human ERBB3 protein (ECD) was obtained from (cat. no. CSB-YP007765HU; Cusabio Technology, LLC) was then added to the CM at a concentration of 100 ng/ml.

Statistical analysis. All experimental data were derived from at least three independent biological replicates and are presented as mean ± SD. Bioinformatic statistics: The correlation between two continuous variables (such as METTL7B and ERBB3 mRNA levels) was assessed using Spearman's rank correlation coefficient. Differences in scRNA-seq cluster marker expression levels were determined using the Wilcoxon rank-sum test. All statistical analyses were performed using GraphPad Prism (v9.0; Dotmatics) or R software (v4.2.0; Posit Software, PBC). $P<0.05$ was considered to indicate a statistically significant difference ($^{*}P<0.05$, $^{**}P<0.01$ and $^{***}P<0.001$). All data are presented as mean ± SD from at least three independent experiments. Statistical differences were analyzed using the unpaired Student's t-test (between two groups) or one-way ANOVA followed by Tukey's post-hoc test.

Results

METTL7B is specifically enriched in malignant epithelial compartment of LUAD. To elucidate the potential non-cell-autonomous roles of METTL7B, the cellular distribution within the LUAD microenvironment was determined. Leveraging the scRNA-seq data from the GSE131907 dataset, 10 major cell lineages via t-SNE visualization were identified (Fig. 1A), and their relative proportions were quantified across specimens (Fig. 1B). The identity of each cluster was confirmed using canonical markers such as surfactant protein C for epithelial cells and CD68 for macrophages (Fig. 1C). Assessment of the METTL7B expression profile across these populations revealed a heterogeneous distribution with a predominant enrichment specifically within the epithelial cell cluster (Fig. 1D). This localization identified METTL7B as a molecular feature of the malignant epithelium. These findings were corroborated by TCGA-LUAD cohort, which demonstrated a marked upregulation of METTL7B in tumor tissues compared with normal controls (Fig. 1E). Collectively, these multi-scale transcriptomic data establish METTL7B as a tumor-specific molecule localized in the malignant epithelium, providing a foundation for investigating its paracrine influence on the immune landscape.

Identification of ERBB3 as a promising molecular associate of METTL7B. To identify the potential molecular associates of METTL7B, differential expression analysis between $METTL7B^{+}$ and $METTL7B^{-}$ epithelial cells was first performed. Significantly upregulated and downregulated genes were identified, including notable transcripts such as tissue factor pathway inhibitor 2, aquaporin 5 and serpin family A member 1 (Fig. 2A). To prioritize candidates with clinical relevance, the correlation between the upregulated differentially expressed genes and METTL7B expression using TCGA-LUAD dataset was evaluated. Spearman's correlation analysis revealed the top ten genes showing the most significant positive association with METTL7B, including ATP binding cassette subfamily C member 3, CD63 and ERBB3 (Fig. 2B). Functional annotation of these ten candidates via GO and Kyoto Encyclopedia of Genes and Genomes enrichment analysis demonstrated their involvement in key biological processes, notably 'ERBB signaling pathway' and the 'MAPK signaling pathway'. (Fig. 2C). To refine this selection, the frequency of participation of each gene in the enriched functional terms was quantified. ERBB3 exhibited the highest involvement frequency, participating in markedly more biological pathways than other candidates (Fig. 2D). Further characterization of ERBB3 expression revealed a pattern highly concordant with that of METTL7B. Single-cell analysis revealed that ERBB3 was predominantly enriched in the epithelial cell population within the TME (Fig. 2E). Consistently, analysis of TCGA-LUAD cohort indicated that ERBB3 expression was significantly elevated in tumor tissues compared with that in normal controls (false discovery rate=1.1×10^{-3}; Fig. 2F). These results identified ERBB3 as a promising candidate for further investigation as a key

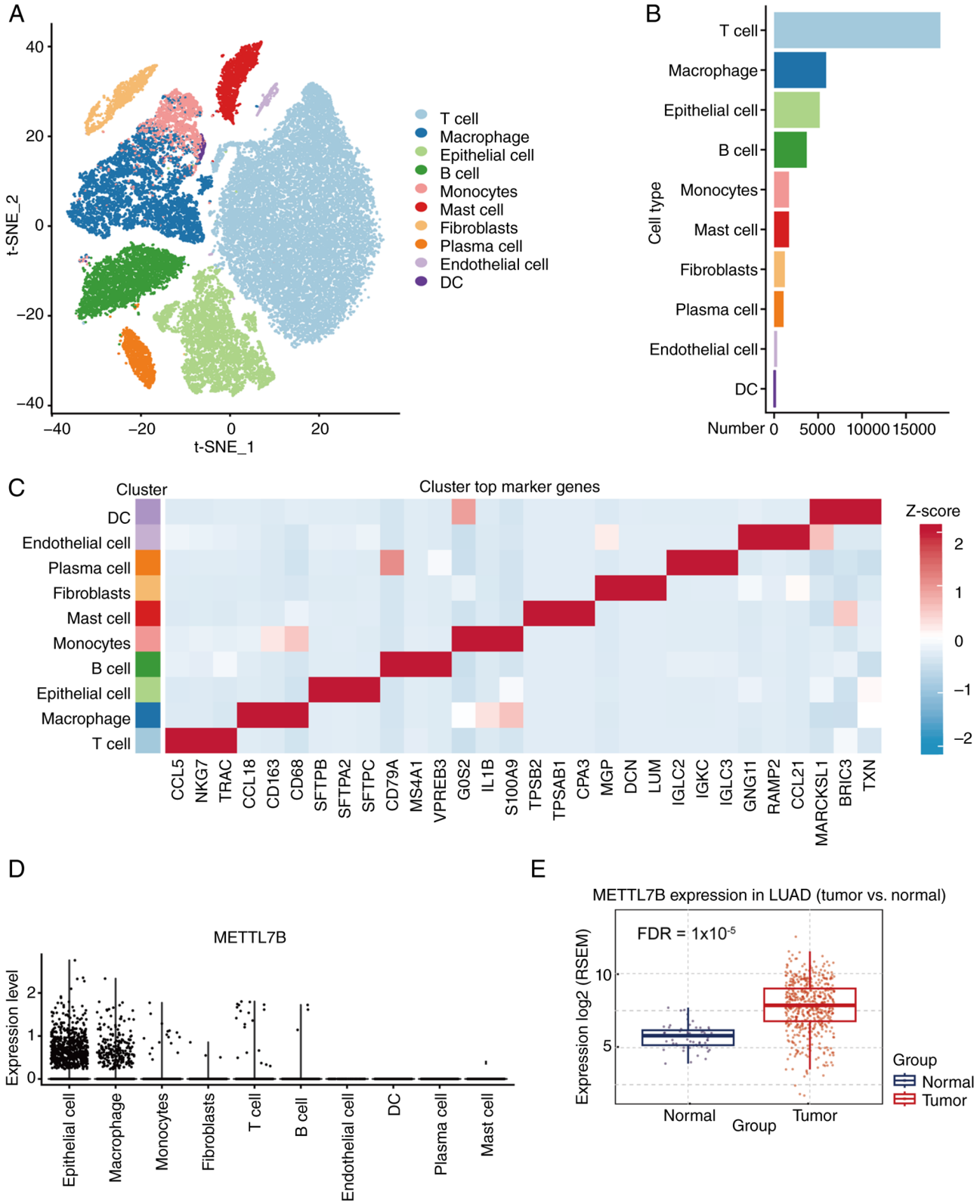

Figure 1. METTL7B is enriched in the malignant epithelial compartment of LUAD. (A) t-SNE visualization of 10 major cell lineages identified in the single cell RNA-sequencing dataset (GSE131907). (B) Bar plot showing the relative proportions of each cell lineage across specimens. (C) Heatmap displaying the expression of canonical marker genes used for cell type annotation. (D) Violin plot depicting the expression levels of METTL7B across different cell populations, showing predominant enrichment in epithelial cells. (E) Box plot comparing METTL7B expression between normal tissues from The Cancer Genome Atlas-LUAD cohort. FDR=1.1x10^{-5}. METTL7B, methyltransferase-like 7B; LUAD, lung adenocarcinoma; DC, dendritic cells; t-SNE, t-distributed stochastic neighbor embedding; FDR, false discovery rate.

molecular associate of METTL7B in LUAD, prompting focus on this axis in subsequent functional studies.

METTL7B and ERBB3^{+} tumor cells exhibit enhanced crosstalk with M2 macrophages. To evaluate the influence

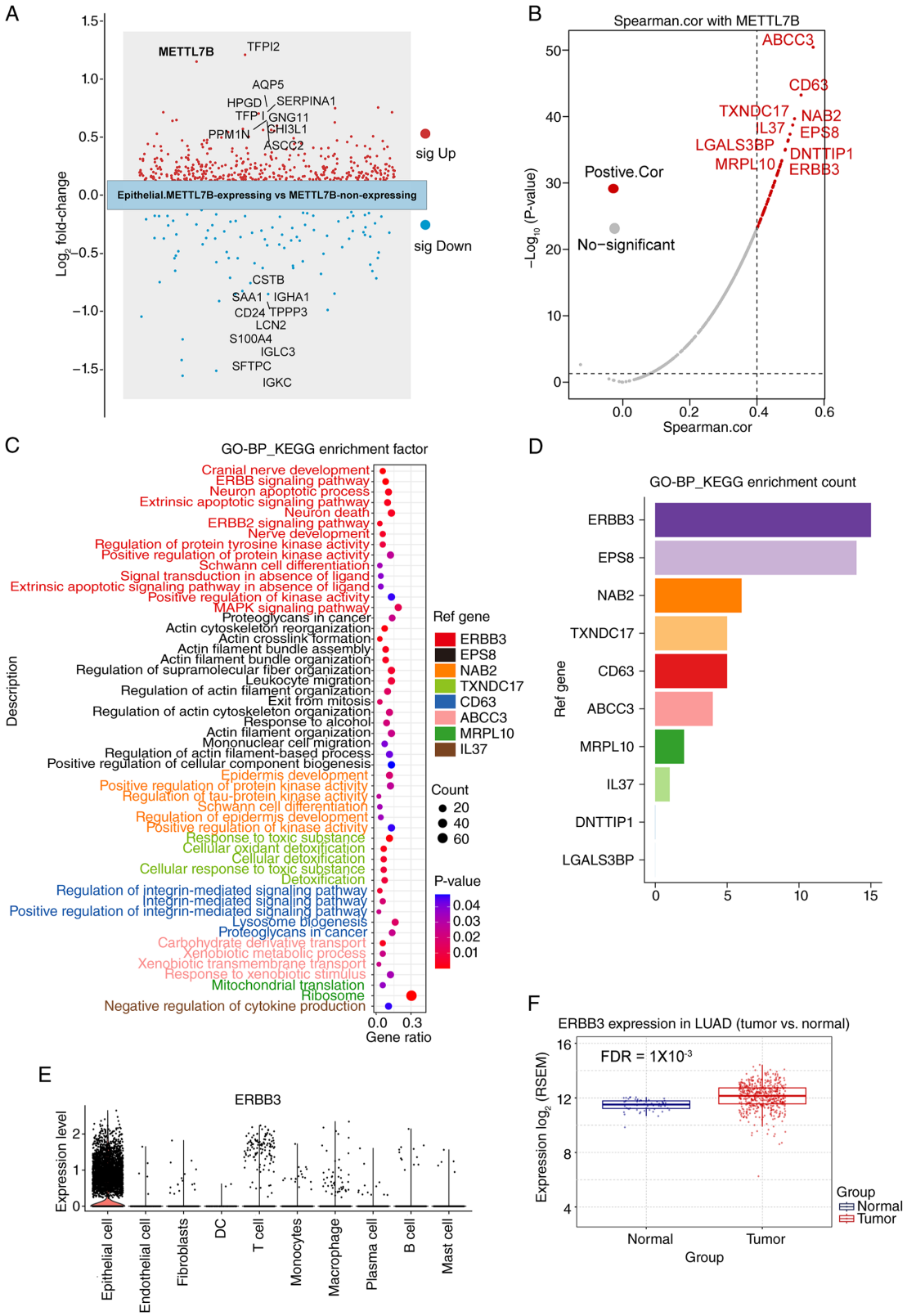

Figure 2. Identification of ERBB3 as a promising molecular associate of METTL7B in LUAD. (A) Volcano plot of DEGs between METTL7B-expressing and METTL7B-non-expressing epithelial cells. Red dots indicate upregulated genes (Log_2 fold change >0.25; P<0.05). (B) Spearman correlation analysis of the top upregulated DEGs with METTL7B expression in TCGA-LUAD dataset. (C) GO and KEGG enrichment analysis of the top 10 METTL7B-associated candidates. (D) Frequency count of candidate genes participating in the enriched biological pathways, identifying ERBB3 as the most involved gene. (E) Violin plot showing ERBB3 expression across different cell lineages in single cell RNA-sequencing data. (F) Box plot comparing ERBB3 expression between normal and tumor tissues in TCGA-LUAD cohort. FDR=$1.1x10^{-3}$. METTL7B, methyltransferase-like 7B; DEGs, differentially expressed genes; TCGA, The Cancer Genome Atlas; LUAD, lung adenocarcinoma; GO, Gene Ontology; BP, biological process; KEGG, Kyoto Encyclopedia of Genes and Genomes; DC, dendritic cell; ERBB3, human epidermal growth factor receptor 3; EPS8, EGFR pathway substrate 8, signaling adaptor; NAB2, NGFI-A binding protein 2; TXNDC17, thioredoxin domain containing 17; ABCC3, ATP binding cassette subfamily C member 3; MRPL10, mitochondrial ribosomal protein L10; DNTTIP1, deoxynucleotidyltransferase terminal interacting protein 1; LGALS3BP, galectin 3 binding protein; sigUP, significantly upregulated; sigDown, significantly downregulated; Cor., correlation; Ref, reference.

of METTL7B and ERBB3 on the LUAD microenvironment, cell-cell communication across the identified cell lineages were modeled. The global interaction network revealed extensive crosstalk among all cell types (Fig. 3A), with epithelial cells exhibiting the strongest interaction, specifically with the macrophages (Fig. 3B). To further characterize this crosstalk, macrophages were sub-clustered into M1 and M2 phenotypes (Fig. 3C), which were validated by the selective enrichment of MRC1 and CD86, respectively (Fig. 3D). Further analysis was performed by stratifying epithelial cells based on the expression of METTL7B or ERBB3. Cell-cell interaction modeling demonstrated that METTL7B$^+$ epithelial cells maintained notably higher interaction weights with M2 macrophages than METTL7B$^-$ cells (Fig. 3G and H). A highly concordant pattern was observed for ERBB3, in which ERBB3$^+$ epithelial cells displayed preferentially enhanced communication with the M2 subpopulation (Fig. 3E and F). These findings indicated that the METTL7B-expressing and ERBB3-high malignant cell states were characterized by intensified interactions with M2 macrophages within the LUAD microenvironment.

METTL7B promotes macrophage recruitment and M2-like polarization in vitro. To investigate the non-cell-autonomous roles of METTL7B *in vitro*, stable METTL7B-KO A549 cells and METTL7B-OE PC9 cell lines were established (Fig. 4A and B). Given that the interaction between tumor cells and macrophages is mediated by extracellular signaling molecules, the effect of METTL7B on key secreted factors was assessed. The expression of METTL7B positively associated with the mRNA levels of the chemoattractants C-C motif chemokine ligand 2 and colony-stimulating factor in both cell lines (Fig. 4C and D). Transwell migration assays demonstrated that CM-derived from METTL7B-high tumor cells notably enhanced the recruitment of U937-derived M0 macrophages, whereas METTL7B deficiency markedly attenuated this chemotactic effect (Fig. 4F and G).

In addition to facilitating macrophage influx, whether METTL7B influenced the functional reprogramming of these cells (Fig. 4H) was evaluated. Phenotypic characterization revealed that METTL7B predominantly triggered an M2-like polarization program, as evidenced by the significant upregulation of M2 markers including CD206, CD163 and ARG-1 (Fig. 4I and J). Notably, in the A549 model, METTL7B KO resulted in a significant increase in the M1-associated markers CD80 and CD86, suggesting a shift in the polarization balance toward an M1-like state upon the loss of METTL7B (Fig. 4I). Conversely, METTL7B OE in PC9 cells specifically induced M2 markers without significantly affecting the M1-associated markers (Fig. 4J). Collectively, these results indicate that METTL7B modulates the tumor-derived paracrine factors to coordinate both the recruitment and immunosuppressive M2-like transition of macrophages *in vitro*.

METTL7B modulates ERBB3 expression and its ADAM10/17-dependent proteolytic ectodomain shedding. Analysis of TCGA LUAD datasets revealed a significant positive correlation between METTL7B and ERBB3 transcript levels (r=0.35; Fig. 5A). RT-qPCR validation showed that METTL7B KO in A549 cells concordantly decreased the mRNA levels of both the full-length (ERBB3-L) and soluble (ERBB3-S) ERBB3 isoforms, whereas ectopic METTL7B overexpression in PC9 cells increased both transcripts (Fig. 5B and C). To rule out passive leakage of ERBB3-ECD from damaged cells, LDH) release assays were performed before quantifying soluble ERBB3 in CM. Basal LDH release remained consistently low in both A549 and PC9 models, and neither METTL7B KO nor OE triggered a significant increase in LDH release relative to the matched controls (Fig. 5D and E), indicating that altered ERBB3-S accumulation is independent of cell death or non-specific membrane leakage. ELISA results showed that ERBB3-S concentrations in the CM were reduced by METTL7B KO in A549 cells and elevated by METTL7B OE in PC9 cells (Fig. 5F and G). Immunoblotting suggested the consistent positive modulation of intracellular ERBB3 protein abundance by METTL7B in both cellular models (Fig. 5H-K). Pretreatment with the ADAM10/17 inhibitor GW280264X for 12 h dose-dependently attenuated the increase in extracellular ERBB3-ECD in both METTL7B KO A549 and OE in PC9 cell models (Fig. 5L and M), suggesting that the increase in ERBB3 ECD release induced by METTL7B is dependent on ADAM metalloproteinase-mediated proteolytic cleavage. Finally, IHC analysis of clinical specimens spanning MIA, IA and LUAD showed gradual upregulation of both METTL7B and ERBB3 during histological progression (Fig. 5N). Quantitative analysis confirmed a positive association with the highest expression levels observed in invasive LUAD (Fig. 5O). These data suggest that the METTL7B-ERBB3 axis is associated with the histological progression of LUAD.

Screening of EGFR as a candidate receptor for ERBB3-S. Candidate receptors mediating the paracrine effect of ERBB3-S on macrophages were screened. The canonical model holds that catalytically impaired ERBB3 transduces intracellular signals via heterodimerization with kinase-active EGFR in epithelial cells (34), consistent with the co-expression of ERBB3 and EGFR in METTL7B$^+$ epithelial cells from the single-cell dataset (Fig. 6A and B). However, ERBB3 expression was negligible in both M1 and M2 macrophages, indicating that the membrane-bound ERBB3-EGFR heterodimer model cannot account for the paracrine action of ERBB3-S on macrophages.

Among ERBB family members, EGFR was expressed at low but detectable levels in macrophages. Protein-protein interaction analysis using the STRING database further predicted a functional association between ERBB3 and EGFR (Fig. 6C). On the basis of its expression profile and predicted interaction potential, EGFR was selected as the candidate receptor for subsequent functional validation.

METTL7B regulates macrophage M2 polarization via the ERBB3-EGFR paracrine axis. Flow cytometry and cytokine profiling was performed to validate the regulatory role of the METTL7B-ERBB3-EGFR paracrine axis in macrophage polarization. In the A549 model, METTL7B KO skewed macrophages toward an M1-like phenotype: Compared with wild-type controls (CD86$^+$, 35.9%; CD206$^+$, 24.0%), KO clones KO-1 and KO-2 showed elevated CD86$^+$ proportions (43.6 and 45.9%) and reduced CD206$^+$ proportions (3.18 and 2.63%; Fig. 7A-C). Supplementation with recombinant ERBB3-S (rERBB3-S) partially rescued this

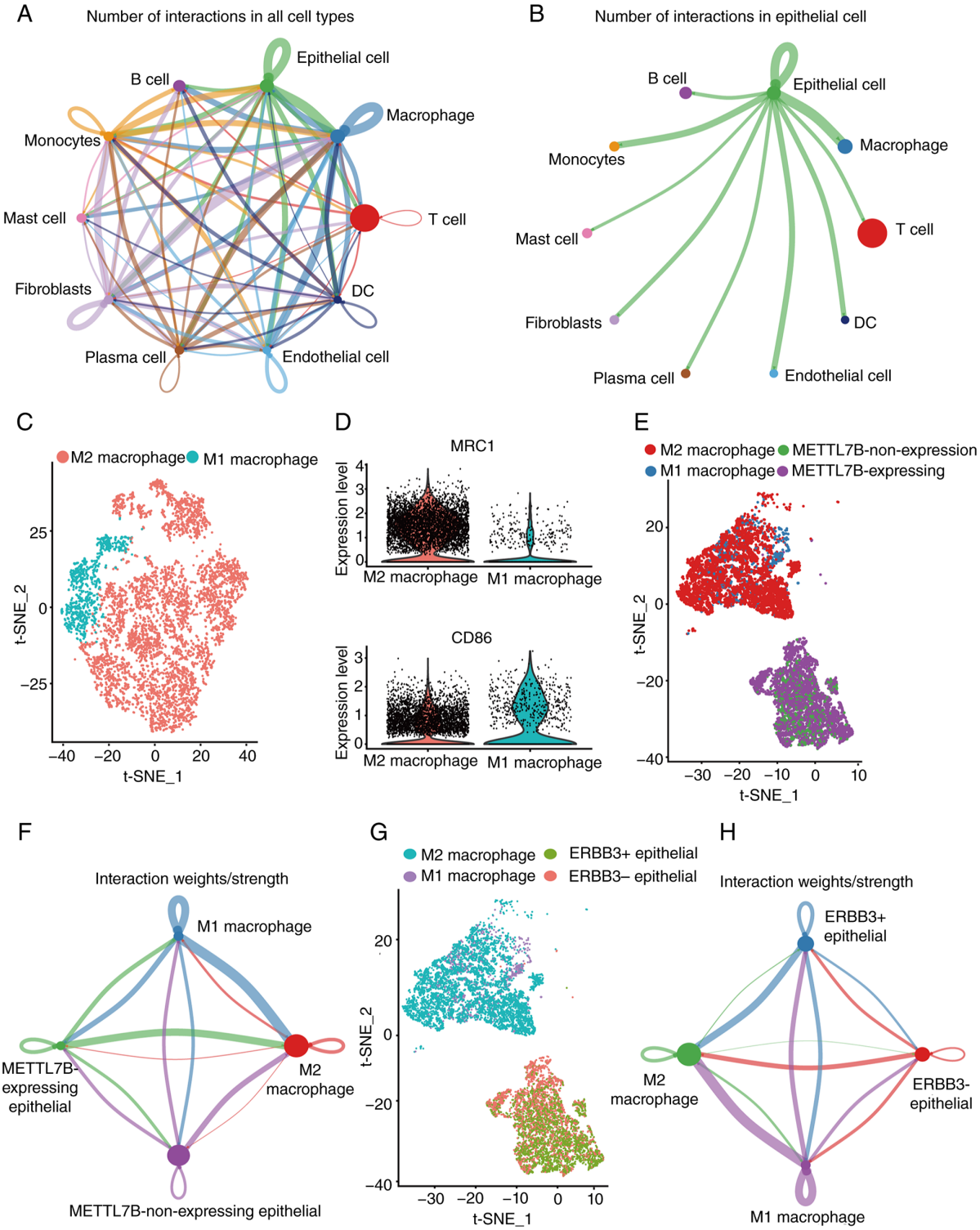

Figure 3. METTL7B$^+$ and ERBB3$^+$ malignant cells exhibit intensified interactions with M2 macrophages. (A) Circle plot visualizing the global cell-cell interaction network across all identified cell types in lung adenocarcinoma. (B) Chord diagram showing specific interaction weights between epithelial cells and other cell populations. (C) t-SNE sub-clustering of the macrophage population into M1 and M2 sub-types. (D) Violin plots of phenotype-specific markers (MRC1 for M2; CD86 for M1) confirming macrophage identity. (E) t-SNE plots showing the distribution of METTL7B+/- malignant epithelial cells. (F) Hierarchy plots quantifying interaction weights/strength between stratified epithelial cells and macrophage sub-clusters(M1 vs. M2). (G) t-SNE plot showing the distribution of ERBB3$^+$/- malignant epithelial cells. (H) Hierarchy plot quantifying interaction weights/strength between ERBB3+/- epithelial cells and macrophage sub-clusters (M1 vs. M2). These plots demonstrate preferential communication between METTL7B$^+$/ERBB3$^+$ tumor cells and M2 macrophages. ERBB3, human epidermal growth factor receptor 3; METTL7B, methyltransferase-like 7B; t-SNE, t-distributed stochastic neighbor embedding; MRC1, mannose receptor C-type 1.

polarization defect, increasing CD206$^+$ and decreasing CD86$^+$ populations relative to the IgG control. EGFR blockade on macrophages substantially attenuated the pro-M2 effect of rERBB3-S, with rebounded CD86$^+$ levels (KO1, 39.3%; KO2,

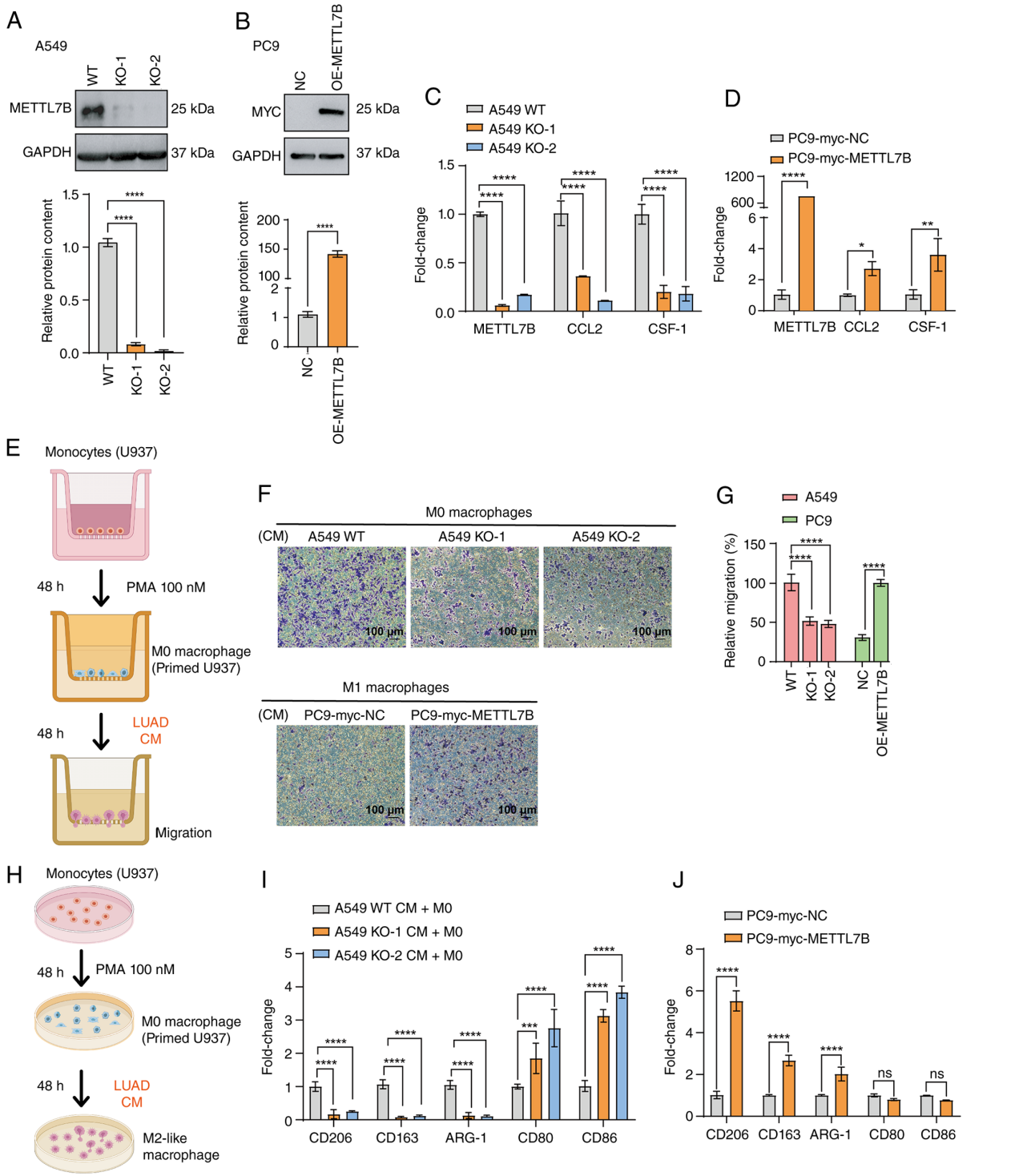

Figure 4. METTL7B promotes macrophage recruitment and M2-like polarization. Western blot confirmation of (A) METTL7B knockout in A549 cells (KO-1 and KO-2) and (B) overexpression in PC9 cells (OE-METTL7B). GAPDH served as the loading control. (C) qPCR analysis of mRNA levels for recruitment factors CCL2 and CSF-1 in METTL7B-knockout A549 cells (WT, KO-1 and KO-2). (D) qPCR analysis of mRNA levels for recruitment factors CCL2 and CSF-1 in METTL7B-overexpressing PC9 cells (NC and OE-METTL7B). (E) Schematic illustration of the transwell macrophage recruitment assay using tumor-CM. (F) Representative images of migrated U937-derived macrophages (crystal violet staining; scale bar, 100 μm). (G) Statistical quantification of relative migration (%). (H) Schematic of the M2 polarization assay. (I) qPCR analysis of M1-associated (CD80 and CD86) and M2-associated (CD206, CD163 and ARG-1) markers in M0 macrophages incubated with CM from (I) wild-type and METTL7B-knockout A549 cells. (J) and incubated with CM from control and METTL7B-overexpressing PC9 cells. Data represent mean ± SD (n=3). *P<0.05, **P<0.01, ***P<0.001, ****P<0.0001. ns, not significant; METTL7B, methyltransferase-like 7B; OE, overexpression; CM, conditioned medium; WT, wild type; NC, negative control; LUAD, lung adenocarcinoma; PMA, phorbol 12-myristate 13-acetate; CCL2, C-C motif chemokine ligand 2; CSF-1, colony-stimulating factor 1; ARG-1, arginase 1; qPCR, quantitative PCR.

34.0%) and reduced CD206^{+} levels (KO-1, 8.68%; KO-2, 11.2%) vs. IgG controls (Fig. 7A-C). Consistent results were observed in the PC9 OE model. METTL7B OE promoted M2-like polarization, reducing the CD86^{+} population from 65.8 to 45.8% and raising the CD206^{+} population from 6.7 to 11.9% (Fig. 7B-D). Pharmacological inhibition of ERBB3 with

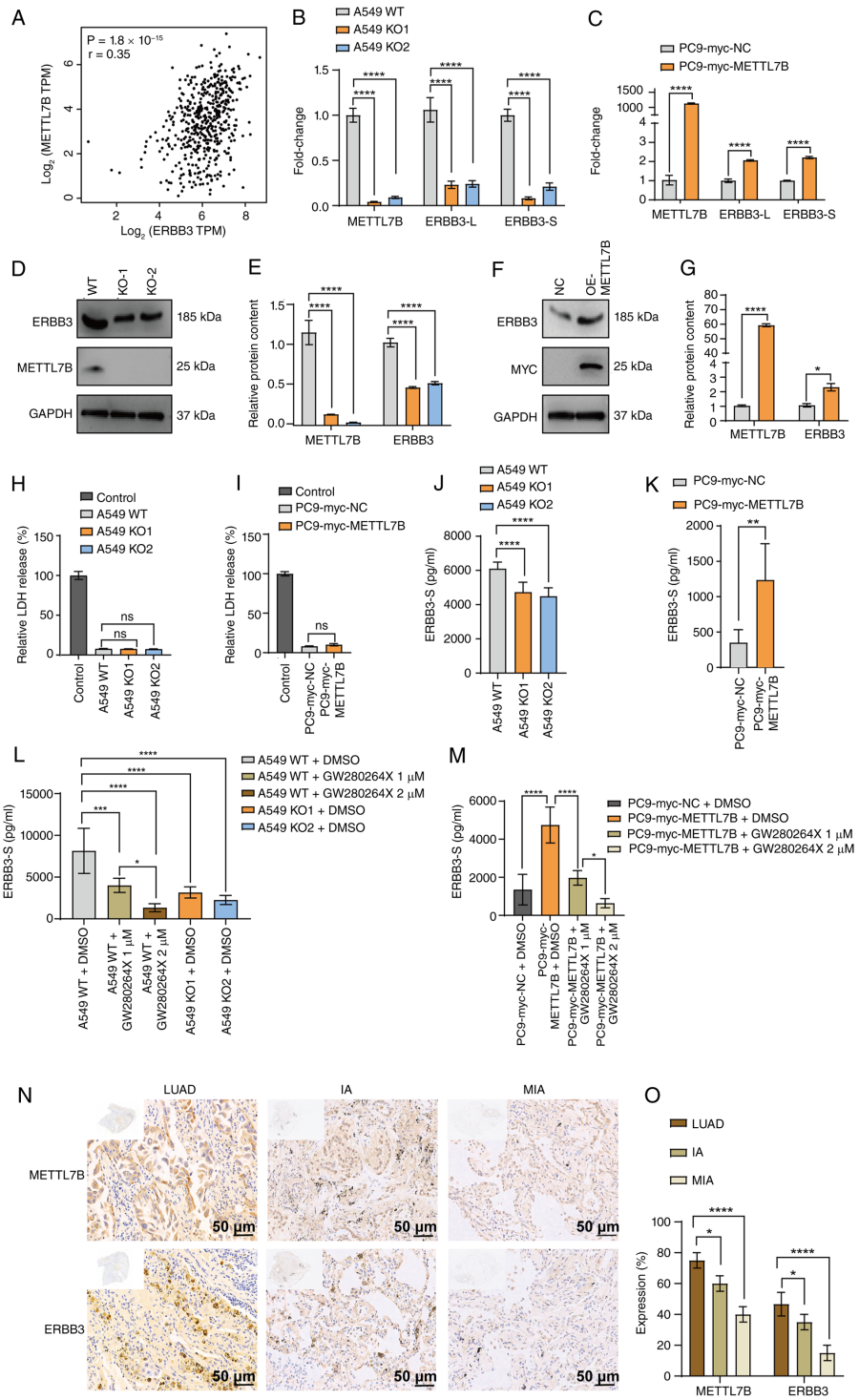

Figure 5. METTL7B modulates ERBB3 expression and its ADAM10/17-dependent proteolytic ectodomain shedding. (A) Pearson correlation analysis of METTL7B and ERBB3 mRNA expression in The Cancer Genome Atlas-LUAD cohort (r=0.35; P=1.8x10^{-15}). Relative transcript levels of METTL7B, ERBB3-L and ERBB3-S in (B) METTL7B-KO A549 cells (KO1, KO2) and (C) METTL7B-OE PC9 cells, determined by quantitative real-time PCR.(D) Western blot detection of intracellular METTL7B and ERBB3 protein levels in METTL7B-knockout A549 cells (KO1, KO2). GAPDH served as the loading control. (E) Densitometric quantification of the western blot results in (D) showing relative protein levels of METTL7B and ERBB3. (F) Western blot detection of intracellular METTL7B (Myc-tagged) and ERBB3 protein levels in METTL7B-OE PC9 cells. GAPDH served as the loading control. (G) Densitometric quantification of the western blot results in (F) showing relative protein levels of METTL7B and ERBB3. (H) LDH release assay to assess cell membrane integrity in METTL7B-knockout A549 cells. (I) LDH release assay to assess cell membrane integrity in METTL7B-OE PC9 cells. ns, not statistically significant. (J) ELISA quantification of ERBB3-S protein concentration in the conditioned medium of METTL7B-KO A549 cells (n=6, from 3 biological replicates and 2 technical replicates). ELISA quantification of ERBB3-S protein concentration in the conditioned medium of (K) METTL7B-OE PC9 cells (n=6). (L) wild-type and METTL7B-KO A549 cells, following 12 h treatment with the ADAM10/17 inhibitor GW280264X at the indicated concentrations. (M) ELISA quantification of ERBB3-S in the conditioned medium of control and METTL7B-OE PC9 cells, following 12 h treatment with the ADAM10/17 inhibitor GW280264X at the indicated concentrations. (N) Immunohistochemical staining of METTL7B and ERBB3 in clinical specimens of LUAD, IA and MIA (scale bar, 50 μm). (O) Quantitative analysis of the percentage of positively stained area (% expression) for METTL7B and ERBB3 across LUAD, IA and MIA specimens. *P<0.05, **P<0.01, ***P<0.001, ****P<0.0001. ns, not significant; METTL7B, methyltransferase-like 7B; ERBB3, human epidermal growth factor receptor 3; WT, wild-type; OE, overexpression; KO, knockout; LDH, lactate dehydrogenase; LUAD, lung adenocarcinoma; MIA, minimally invasive adenocarcinoma; IA, invasive adenocarcinoma; ERBB3-S, soluble ERBB3; ERBB3-L, full length ERBB3; ADAM10/17, ADAM metallopeptidase domain 10/17.

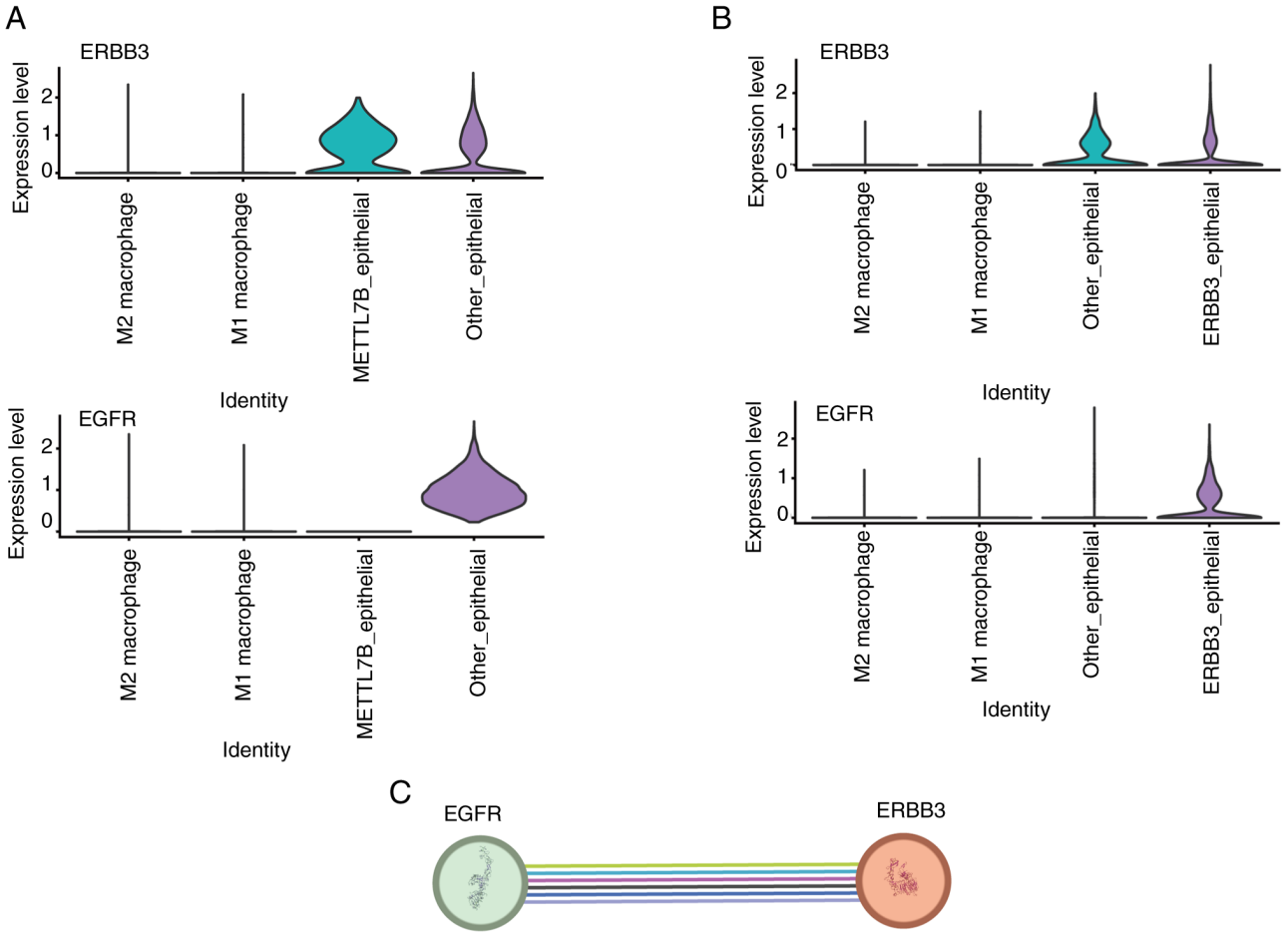

Figure 6. Expression landscape and protein interaction prediction identify EGFR as a candidate receptor for soluble ERBB3 in macrophages. (A) Violin plots showing the single-cell expression distribution of ERBB3 and EGFR across M2 macrophages, M1 macrophages, METTL7B$^+$ epithelial cells and other epithelial cells. (B) Violin plots displaying the expression of ERBB3 and EGFR in M2 macrophages, M1 macrophages, other epithelial cells and ERBB3$^+$ epithelial cells at single-cell resolution. (C) Protein-protein interaction analysis derived from the STRING database, showing the predicted functional association between ERBB3 and EGFR. ERBB3, human epidermal growth factor receptor 3; METTL7B, methyltransferase-like 7B.

TX1-85-1 partially reversed this phenotype, restoring CD86$^+$ to 61.0% and lowering CD206$^+$ to 9.85%.

Cytokine profiling of co-culture supernatants was concordant with surface marker changes. In the A549 model, METTL7B KO decreased M2-associated IL-10 and TGF-β and increased M1-related IL-12 and TNF-α; rERBB3-S partially restored the cytokine profile, while EGFR blockade attenuated this rescue effect (Fig. 7E-H). In the PC9 model, METTL7B OE elevated IL-10 and TGF-β and suppressed IL-12 and TNF-α, which was partially reversed by TX1-85-1 (Fig. 7I-L). Collectively, these data support that METTL7B promotes functional M2 macrophage polarization via the ERBB3-EGFR paracrine axis.

Discussion

Orchestration of the immunosuppressive niche is a fundamental hallmark of LUAD progression. The present study demonstrated that METTL7B functions as a key non-cell-autonomous regulator of macrophage functional states. By integrating high-resolution single-cell transcriptomic insights with functional *in vitro* validation, the present study demonstrated that METTL7B influences macrophage M2-like polarization by facilitating the expression and extracellular release of the ERBB3-S ECD. Clinically, IHC analysis demonstrated that METTL7B and ERBB3 expression progressively increased with histological progression from MIA to IA. This trend suggests that activation of the METTL7B-ERBB3 signaling axis may represent a key transition from cell-intrinsic oncogenic growth to active microenvironment remodeling. By upregulating and releasing ERBB3-ECD during the early stages of invasion, malignant cells may effectively precondition the immune soil, thereby fostering an M2-rich niche that facilitates subsequent tumor expansion and immune evasion. The potential 're-purposing' of ERBB3 within the LUAD microenvironment represents a marked shift from its canonical role.

Traditionally, ERBB3 has been characterized as a transmembrane 'pseudokinase' that mediates bypass signaling and therapy resistance (35,36). Consistent with the emerging theoretical framework proposed by Li *et al* (36), the present data supports ERBB3 as a multifunctional signaling hub with paracrine activity beyond its canonical cell-intrinsic role. In the present study METTL7B positively regulated both total ERBB3 expression and the extracellular availability of ERBB3-ECD. Notably, rescue assays showed that

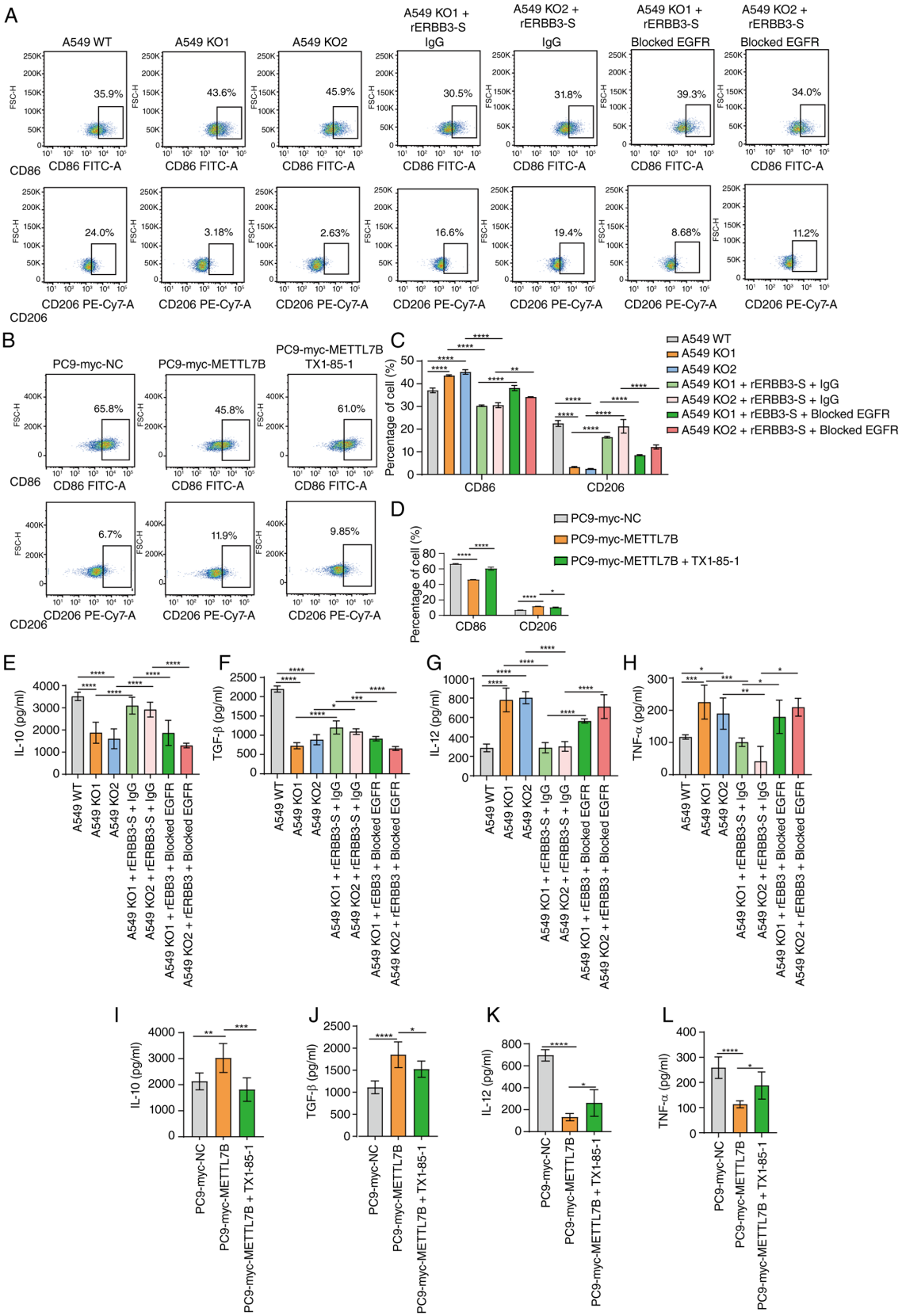

Figure 7. Rescue and blockade assays verify that METTL7B promotes functional M2 macrophage polarization via the ERBB3-EGFR paracrine axis. (A) Representative flow cytometry plots of CD86 (M1 marker) and CD206 (M2 marker) in macrophages treated with conditioned medium from wild-type A549 cells, METTL7B-KO A549 cells and METTL7B-KO A549 cells supplemented with rERBB3-S plus IgG control or EGFR blockade (10 μg/ml). (B) Representative flow cytometry plots of CD86 and CD206 in macrophages treated with conditioned medium from control PC9 cells, METTL7B-OE PC9 cells and METTL7B-OE PC9 cells treated with the ERBB3 inhibitor TX1-85-1 (5 μM). (C) Quantitative analysis of CD86+ and CD206+ macrophage proportions in (C) A549 cell model. (D) in the PC9 cell model. ELISA quantification of M2-associated immunosuppressive cytokines (E) IL-10, (F) TGF-β and M1-associated pro-inflammatory cytokines (G) IL-12 and (H) TNF-α in co-culture supernatants from the A549 cell model. ELISA quantification of (I) IL-10, (J) TGF-β, (K) IL-12 and (L) TNF-α in co-culture supernatants from the PC9 cell model. *P<0.05, **P<0.01, ***P<0.001 and ****P<0.0001. ERBB3, human epidermal growth factor receptor 3; OE, overexpression; WT, wild-type; KO, knockout; rERBB3-S, recombinant human ERBB3-S; ERBB3-S, soluble ERBB3.

supplementation with r-ERBB3-ECD partially reversed the M1-skewed phenotype caused by the METTL7B KO, reduced CD86 expression and restored CD206 levels. Cytokine profiling further validated functional reprogramming, with ERBB3-ECD increasing M2-associated IL-10 and TGF-β while decreasing M1-related IL-12 and TNF-α secretion. Furthermore, EGFR blockade in macrophages substantially attenuated the phenotypic and functional changes induced by ERBB3-ECD. Together with the detectable EGFR expression in macrophages and the predicted protein-protein interactions, these data support EGFR as a candidate receptor mediating the paracrine effect of ERBB3-ECD on macrophage polarization.

These findings have important implications in ERBB3-targeted therapies. Current clinical strategies, particularly ADCs, such as patritumab deruxtecan (HER3-DXd) (22,23,37,38), rely on the precise recognition of membrane-bound ERBB3 to deliver cytotoxic payloads (26). However, in the present study, observation of detectable levels of ERBB3-ECD in the extracellular space suggests a potential mechanism of for 'antigen interception'. This phenomenon mirrors observations in other ErbB family members, such as HER2 (36,39). Clinical and mechanistic evidence has demonstrated that the expression of truncated HER2 fragments and the subsequent shedding of the ECD can sequester therapeutic antibodies such as trastuzumab, thereby diminishing their binding to membrane-bound targets and fostering therapy resistance (40,41). It has been further elucidated that this ectodomain shedding not only acts as a physical 'decoy' to neutralize targeted agents but also actively promotes a broader immunosuppressive environment and systemic therapeutic resistance (42,43). Analogously, METTL7B-mediated ERBB3-ECD release may represent a mechanism for both immune evasion and resistance to ERBB3-targeted therapy in LUAD.

The mechanism of ERBB3-ECD release was investigated, focusing on the modulation of proteolytic shedding-a process typically mediated by 'molecular scissors' such as the ADAM (a disintegrin and metalloproteinase) family, specifically ADAM10 or ADAM17 (41,43). Using pharmacological inhibition, the present study demonstrated that ERBB3-ECD release was dependent on ADAM10/17-mediated proteolytic cleavage and ADAM10/17 inhibitors significantly reduced ERBB3-S ECD levels in both METTL7B-OE PC9 and wild-type A549 cells. The combination of ADAM inhibitors and HER3-targeted ADCs may be a viable strategy. This is consistent with the established role of ADAM proteases in mediating ectodomain shedding by other ErbB family members (42). However, the contribution of alternatively spliced secreted ERBB3 isoforms cannot be excluded, which lack a transmembrane anchor due to alternative splicing (42,44). The combination of ADAM inhibitors with ERBB3-targeted therapies may represent a key therapeutic strategy. However, the precise mechanism through which METTL7B upregulates ERBB3-L remains unclear. As a member of the methyltransferase-like protein family, METTL7B may regulate ERBB3 through m^6A-dependent mechanisms, similar to METTL3 (16,45). For example, ERBB3 mRNA can be modified to enhance its stability or regulate ADAM protease expression post-transcriptionally. Defining whether METTL7B modulates ERBB3 via m^6A methylation is an important direction for future work.

Several limitations of the present study should be acknowledged. Mechanistically, although EGFR was identified as a candidate receptor for ERBB3-S on macrophages, the precise binding interface between ERBB3-ECD and EGFR, as well as the downstream intracellular signaling cascades that drive M2 polarization, remain to be fully elucidated. Additionally, other potential binding partners of soluble ERBB3 on macrophages cannot be fully excluded and warrant further investigation. Likewise, the upstream mechanism by which METTL7B upregulates ERBB3, particularly the potential involvement of m^6A methylation, awaits rigorous validation via methylated RNA immunoprecipitation-sequencing and methyltransferase-dead mutant rescue assays. Functionally, the conclusion of M2-like macrophage polarization is supported by surface marker profiling and cytokine secretion analyses; however, direct functional evidence of immunosuppressive capacity, such as from T cell suppression assays, has not yet been established. Furthermore, all functional data were generated *in vitro*. The pathophysiological role of the METTL7B-ERBB3-EGFR paracrine axis within the complex, three-dimensional TME requires *in vivo* validation. Ongoing and future work should prioritize this direction using both syngeneic murine lung cancer models and humanized immune system mouse models, complemented by patient-derived xenografts and *in vivo* therapeutic intervention studies. Finally, while the present IHC data demonstrate a progressive increase in METTL7B and ERBB3 expression along LUAD histological progression, larger independent clinical cohorts and spatial transcriptomic analyses are warranted to further validate the clinical relevance and prognostic value of this axis.

In summary, the present study defines a METTL7B-ERBB3-EGFR paracrine axis that drives M2-like macrophage polarization in LUAD. METTL7B upregulates ERBB3 expression, and the release of ERBB3 ectodomain is dependent on ADAM10/17-mediated proteolytic cleavage; soluble ERBB3-ECD then acts on macrophages via EGFR to induce functional M2 reprogramming. These findings expand understanding of the non-cell autonomous functions of METTL7B and highlight the METTL7B-ERBB3 axis as a potential therapeutic target for LUAD.

Acknowledgements

The authors would like to thank Ms. Fuhua Zhong (Department of Central Laboratory, Shenzhen People's Hospital, Guangdong, China) for technical guidance on the construction of A549 METTL7B knockout cell lines.

Funding

The present study was supported by the National Natural Science Foundation of China (grant no. 82372751), Shenzhen Medical Research Fund (grant no. A2403067), Guangdong Basic and Applied Basic Research Foundation (grant no. 2025A1515220203), Science and Technology Foundation of Shenzhen (grant no. SGCX20250526154203004) and Shenzhen People's Hospital Physician Scientist Training 'Five Three Program' (grant no. SYWGSJCYJ202303).

Availability of data and materials

The data generated in the present study may be requested from the corresponding author.

Authors' contributions

SH conceived and designed the study, performed the experiments, analyzed and interpreted the data, and wrote the manuscript. HS analyzed and interpreted the data, and edited the manuscript. JW performed the experiments and analyzed the data. JX performed the experiments, and contributed to data analysis and interpretation. NL and JC performed the experiments and analyzed the data. ZZ performed the experiments and analyzed the data. XC conceptualized and designed the study, analyzed and interpreted the data, and edited the manuscript. CZ conceptualized and designed the study, supervised the experiments, analyzed and interpreted the data, and edited the manuscript. All authors have read and approved the final manuscript. SH and CZ confirm the authenticity of all the raw data.

Ethics approval and consent to participate

The study was conducted in accordance with the Declaration of Helsinki, and approved by the Clinical Research Ethics Committee of Shenzhen People's Hospital (approval no. LL-KY-2024161-01; approval date: 2024-10-18). Written informed consent was obtained from all patients for the use of their residual formalin-fixed paraffin-embedded lung adenocarcinoma tissue specimens in the present study.

Patient consent for publication

Not applicable.

Competing interests

The authors declare that they have no competing interests.

References

1. Zhang Y, Vaccarella S, Morgan E, Li M, Etxeberria J, Chokunonga E, Manraj SS, Kamate B, Omonisi A and Bray F: Global variations in lung cancer incidence by histological subtype in 2020: A population-based study. Lancet Oncol 24: 1206-1218, 2023.
2. Bray F, Laversanne M, Sung H, Ferlay J, Siegel RL, Soerjomataram I and Jemal A: Global cancer statistics 2022: GLOBOCAN estimates of incidence and mortality worldwide for 36 cancers in 185 countries. CA Cancer J Clin 74: 229-263, 2024.
3. Su PL, Furuya N, Asrar A, Rolfo C, Li Z, Carbone DP and He K: Recent advances in therapeutic strategies for non-small cell lung cancer. J Hematol Oncol 18: 35, 2025.
4. Borgeaud M, Olivier T, Bar J, Saw SPL, Parikh K, Banna GL, De Vito C, Feldman J, Le X and Addeo A: Personalized care for patients with EGFR-mutant nonsmall cell lung cancer: Navigating early to advanced disease management. CA Cancer J Clin 75: 387-409, 2025.
5. Spigel DR, Faivre-Finn C, Gray JE, Vicente D, Planchard D, Paz-Ares L, Vansteenkiste JF, Garassino MC, Hui R, Quantin X, *et al*: Five-year survival outcomes from the PACIFIC Trial: Durvalumab after chemoradiotherapy in stage III non-small-cell lung cancer. J Clin Oncol 40: 1301-1311, 2022.
6. Binnewies M, Roberts EW, Kersten K, Chan V, Fearon DF, Merad M, Coussens LM, Gabrilovich DI, Ostrand-Rosenberg S, Hedrick CC, *et al*: Understanding the tumor immune microenvironment (TIME) for effective therapy. Nat Med 24: 541-550, 2018.
7. Cheng Y, Zhang T and Xu Q: Therapeutic advances in non-small cell lung cancer: Focus on clinical development of targeted therapy and immunotherapy. MedComm (2020) 2: 692-729, 2021.
8. Sharma P, Hu-Lieskovan S, Wargo JA and Ribas A: Primary, adaptive, and acquired resistance to cancer immunotherapy. Cell 168: 707-723, 2017.
9. Toledo B, Zhu Chen L, Paniagua-Sancho M, Marchal JA, Perán M and Giovannetti E: Deciphering the performance of macrophages in tumour microenvironment: A call for precision immunotherapy. J Hematol Oncol 17: 44, 2024.
10. Noy R and Pollard JW: Tumor-associated macrophages: From mechanisms to therapy. Immunity 41: 49-61, 2014.
11. Chen S, Saeed AFUH, Liu Q, Jiang Q, Xu H, Xiao GG, Rao L and Duo Y: Macrophages in immunoregulation and therapeutics. Signal Transduct Target Ther 8: 207, 2023.
12. Waibl Polania J, Hoyt-Miggelbrink A, Tomaszewski WH, Wachsmuth LP, Lorrey SJ, Wilkinson DS, Lerner E, Woroniecka K, Finlay JB, Ayasoufi K and Fecci PE: Antigen presentation by tumor-associated macrophages drives T cells from a progenitor exhaustion state to terminal exhaustion. Immunity 58: 232-246.e6, 2025.
13. Do MH, Shi W, Ji L, Ladewig E, Zhang X, Srivastava RM, Capistrano KJ, Edwards C, Malik I, Nixon BG, *et al*: Reprogramming tumor-associated macrophages to outcompete endovascular endothelial progenitor cells and suppress tumor neoangiogenesis. Immunity 56: 2555-2569.e5, 2023.
14. Xu J, Ding L, Mei J, Hu Y, Kong X, Dai S, Bu T, Xiao Q and Ding K: Dual roles and therapeutic targeting of tumor-associated macrophages in tumor microenvironments. Signal Transduct Target Ther 10: 268, 2025.
15. Pittet MJ, Michielin O and Migliorini D: Clinical relevance of tumour-associated macrophages. Nat Rev Clin Oncol 19: 402-421, 2022.
16. Qi YN, Liu Z, Hong LL, Li P and Ling ZQ: Methyltransferase-like proteins in cancer biology and potential therapeutic targeting. J Hematol Oncol 16: 89, 2023.
17. Liu D, Li W, Zhong F, Yin J, Zhou W, Li S, Sun X, Xu J, Li G, Wen Y, *et al*: METTL7B Is required for cancer cell proliferation and tumorigenesis in non-small cell lung cancer. Front Pharmacol 11: 178, 2020.
18. Song H, Liu D, Wang L, Liu K, Chen C, Wang L, Ren Y, Ju B, Zhong F, Jiang X, *et al*: Methyltransferase like 7B is a potential therapeutic target for reversing EGFR-TKIs resistance in lung adenocarcinoma. Mol Cancer 21: 43, 2022.
19. Yarden Y and Sliwkowski MX: Untangling the ErbB signalling network. Nat Rev Mol Cell Biol 2: 127-137, 2001.
20. Murtuza A, Bulbul A, Shen JP, Keshavarzian P, Woodward BD, Lopez-Diaz FJ, Lippman SM and Husain H: Novel third-generation EGFR tyrosine kinase inhibitors and strategies to overcome therapeutic resistance in lung cancer. Cancer Res 79: 689-698, 2019.
21. Jura N, Endres NF, Engel K, Deindl S, Das R, Lamers MH, Wemmer DE, Zhang X and Kuriyan J: Mechanism for activation of the EGF receptor catalytic domain by the juxtamembrane segment. Cell 137: 1293-1307, 2009.
22. Yu HA, Goto Y, Hayashi H, Felip E, Chih-Hsin Yang J, Reck M, Yoh K, Lee SH, Paz-Ares L, Besse B, *et al*: HERTHENA-Lung01, a phase II trial of patritumab deruxtecan (HER3-DXd) in epidermal growth factor receptor-mutated non-small-cell lung cancer after epidermal growth factor receptor tyrosine kinase inhibitor therapy and platinum-based chemotherapy. J Clin Oncol 41: 5363-5375, 2023.
23. Yonesaka K, Tanizaki J, Maenishi O, Haratani K, Kawakami H, Tanaka K, Hayashi H, Sakai K, Chiba Y, Tsuya A, *et al*: HER3 augmentation via blockade of EGFR/AKT signaling enhances anticancer activity of HER3-Targeting patritumab deruxtecan in EGFR-Mutated non-small cell lung cancer. Clin Cancer Res 28: 390-403, 2022.
24. Soltoff SP, Carraway KL III, Prigent SA, Gullick WG and Cantley LC: ErbB3 is involved in activation of phosphatidylinositol 3-kinase by epidermal growth factor. Mol Cell Biol 14: 3550-3558, 1994.
25. Garrett JT, Tendler S, Feroz W, Kilroy MK and Yu H: Emerging importance of HER3 in tumorigenesis and cancer therapy. Nat Rev Clin Oncol 22: 348-370, 2025.

26. Ma Y, Huang Y, Zhao Y, Zhao S, Xue J, Yang Y, Fang W, Guo Y, Han Y, Yang K, *et al*: BL-B01D1, a first-in-class EGFR-HER3 bispecific antibody-drug conjugate, in patients with locally advanced or metastatic solid tumours: A first-in-human, open-label, multicentre, phase 1 study. Lancet Oncol 25: 901-911, 2024.
27. Roskoski R Jr: The ErbB/HER family of protein-tyrosine kinases and cancer. Pharmacol Res 79: 34-74, 2014.
28. Haikala HM and Jänne PA: Thirty years of HER3: From basic biology to therapeutic interventions. Clin Cancer Res 27: 3528-3539, 2021.
29. Engelman JA, Zejnullahu K, Mitsudomi T, Song Y, Hyland C, Park JO, Lindeman N, Gale CM, Zhao X, Christensen J, *et al*: MET amplification leads to gefitinib resistance in lung cancer by activating ERBB3 signaling. Science 316: 1039-1043, 2007.
30. Chan G, Nogalski MT and Yurochko AD: Activation of EGFR on monocytes is required for human cytomegalovirus entry and mediates cellular motility. Proc Natl Acad Sci USA 106: 22369-22374, 2009.
31. Zhao G, Liu L, Peek RM Jr, Hao X, Polk DB, Li H and Yan F: Activation of epidermal growth factor receptor in macrophages mediates feedback inhibition of M2 polarization and gastrointestinal tumor cell growth. J Biol Chem 291: 20462-20472, 2016.
32. Kim N, Kim HK, Lee K, Hong Y, Cho JH, Choi JW, Lee JI, Suh YL, Ku BM, Eum HH, *et al*: Single-cell RNA sequencing demonstrates the molecular and cellular reprogramming of metastatic lung adenocarcinoma. Nat Commun 11: 2285, 2020.
33. Livak KJ and Schmittgen TD: Analysis of relative gene expression data using real-time quantitative PCR and the 2(-Delta Delta C(T)) Method. Methods 25: 402-408, 2001.
34. Desai O, Rathore M, Boutros CS, Wright M, Bryson E, Curry K and Wang R: HER3: Unmasking a twist in the tale of a previously unsuccessful therapeutic pursuit targeting a key cancer survival pathway. Genes Dis 12: 101354, 2024.
35. Li Y, Liu Z, Zhao Y, Yang J, Xiao TS, Conlon RA and Wang Z: PD-L1 expression is regulated by ATP-binding of the ERBB3 pseudokinase domain. Genes Dis 10: 1702-1713, 2022.
36. Li Y, Wang Z, Gu M, Huang F and Chang P: HER3 beyond the canonical paradigm: A versatile signaling hub in oncogenesis and therapeutic resistance. J Transl Med 24: 554, 2026.
37. Yu HA, Baik C, Kim DW, Johnson ML, Hayashi H, Nishio M, Yang JC, Su WC, Gold KA, Koczywas M, *et al*: Translational insights and overall survival in the U31402-A-U102 study of patritumab deruxtecan (HER3-DXd) in EGFR-mutated NSCLC. Ann Oncol 35: 437-447, 2024.
38. Fuereder T, Garde-Noguera J, García-Mosquera JJ, Ruiz-Borrego M, Valero M, Llombart-Cussac A, Gion M, Greil R, Arumi M, Campolier M, *et al*: Patritumab deruxtecan (HER3-DXd) in patients with active brain metastases of non-small-cell lung cancer (TUXEDO-3): A multicentre, single-arm, phase 2 trial. Lancet Oncol 26: 1454-1466, 2025.
39. Pernas S and Tolaney SM: HER2-positive breast cancer: New therapeutic frontiers and overcoming resistance. Ther Adv Med Oncol 11: 1758835919833519, 2019.
40. Scaltriti M, Rojo F, Ocaña A, Anido J, Guzman M, Cortes J, Di Cosimo S, Matias-Guiu X, Ramon Y Cajal S, Arribas J, *et al*: Expression of p95HER2, a truncated form of the HER2 receptor, and response to anti-HER2 therapies in breast cancer. J Natl Cancer Inst 99: 628-638, 2007.
41. Arora S, Scott AM and Janes PW: ADAM proteases in cancer: Biological roles, therapeutic challenges, and emerging opportunities. Cancers (Basel) 17: 1703, 2025.
42. Yang Y, Gao Y, Cui H, Li S, Qi Z, Wang Z, Li D, Chen L, Feng M, Wu X, *et al*: Oligodendrocyte-secreted ERBB3 mediates the competitive uptake of copper ions by tumor cells to promote brain metastasis in lung cancer. Int J Biol Sci 22: 3580-3599, 2026.
43. Gnosa SP, Puig Blasco L, Piotrowski KB, Freiberg ML, Savickas S, Madsen DH, Auf Dem Keller U, Kronqvist P and Kveiborg M: ADAM17-mediated EGFR ligand shedding directs macrophage-promoted cancer cell invasion. JCI insight 7: e155296, 2022.
44. Lee H and Maihle NJ: Isolation and characterization of four alternate c-erbB3 transcripts expressed in ovarian carcinoma-derived cell lines and normal human tissues. Oncogene 16: 3243-3252, 1998.
45. Zeng C, Huang W, Li Y and Weng H: Roles of METTL3 in cancer: Mechanisms and therapeutic targeting. J Hematol Oncol 13: 117, 2020.